JOURNAL OF BACTERIOLOGY, Apr. 1982, p. 348–357
0021-9193/82/040348-10$02.00/0

Vol. 150, No. 1

Structure of the Regular Surface Layer of *Aquaspirillum serpens* MW5

MURRAY STEWART[1,2]†* AND R. G. E. MURRAY[2]

Commonwealth Scientific and Industrial Research Organization, Division of Computing Research, Canberra City, ACT 2601, Australia,[1] and Department of Microbiology and Immunology, Faculty of Medicine, University of Western Ontario, London, Ontario, Canada N6A 5C1[2]

Received 3 August 1981/Accepted 6 November 1981

The structure of the regular surface layer of *Aquaspirillum serpens* MW5 has been investigated by electron microscopy supplemented by computer image processing and least-squares analysis. The layer has a ribbed appearance, both on the bacterium and in isolated, negatively stained fragments. However, detailed analysis indicated that the layer was composed of two hexagonal sheets having *p6mm* symmetry and $a = 16$ nm. One sheet was staggered by one half repeat along a (1,0) line of the *p6mm* lattice relative to the second so that, in projection, the pattern of the composite layer was a translational moiré, characterized by a series of ribs spaced 16 nm apart. The ribbed layer had *cmm* symmetry with $a = 32$ nm and $b = 18.5$ nm. Analysis of this pattern indicated that the two *p6mm* hexagonal sheets were unevenly stained, and this was confirmed by using least-squares methods to simulate the observed pattern by combining two hexagonal patterns. The general structure of the layer was consistent with a role as a selective and protective barrier on the cell surface.

The regular arrays of protein units found on the outermost surface of many gram-positive and -negative bacteria (reviewed in references 3 and 14) are of considerable interest because they represent the interface between the cell and its environment. These regular surface (or RS) layers often possess a high degree of structural regularity, which makes them excellent vehicles for the study of macromolecular assembly and arrangement, particularly when electron microscopy and image processing techniques are employed (1, 3, 11, 12, 14–18). RS layers are generally constructed from a single protein species that assembles into either hexagonal or tetragonal patterns which cover the entire cell surface. A principal function of these RS layers appears to be related to protecting the bacterium from hostile environmental agents (reviewed in reference 3). In this context, it has been proposed that the gaps or holes generally present in the layer may be important in that they are sufficiently large to allow the free exchange of small molecules (such as nutrients and waste products) between the cell and its environment, while being sufficiently small to screen the cell from large molecules, such as lytic enzymes and plasmids (16, 17).

The structure of the RS layer of several strains of *Aquaspirillum serpens* has been investigated. Many of these layers have a hexagonal pattern consisting of distinct annuli connected by fine linkers (3, 6–8, 12). Two different linker conformations have been observed. *A. serpens* VHA has "Y" linkers, directed along the (1,1) lines of the hexagonal lattice (6–8, 12), whereas other strains (such as strain MW6) have "delta" linkers directed along the (1,0) lattice lines. The RS layer of *A. serpens* MW5 is somewhat unusual in that it generally shows a ribbed appearance. We have now investigated the structure of this layer in detail to a nominal resolution of 2.5 nm by using electron microscopy and computer image processing. These results, supplemented by quantitative least-squares analysis, have permitted the structure of this layer to be defined and related to the structure of its constituents and also to the structure of related RS layers in other *A. serpens* strains.

MATERIALS AND METHODS

Culture conditions. *A. serpens* MW5 (University of Western Ontario Culture Collection no. 377) was grown at 30°C in a medium consisting of 0.1% yeast extract, 0.1% peptone (both from Difco, Detroit, Mich.), 0.05% anhydrous sodium acetate, 0.0005% L-cysteine, and 0.025% $MgSO_4 \cdot 7H_2O$ adjusted to pH 7.6 with NaOH. After autoclaving, sterile $CaCl_2 \cdot 2H_2O$ was added to give a final concentration of 0.025%. Solid medium was made as required by the addition of 1.5% agar (Bacto-Agar; Difco). Cultures of *A. serpens* MW5 in fluid medium were incubated and swirled

† Present address: MRC Laboratory of Molecular Biology, Cambridge CB2 2QH, England.

(Gyratory shaker; New Brunswick Scientific Co., New Brunswick, N.J.) for 18 to 24 h.

Preparation and examination of specimens. Fixation and embedding were carried out both on whole cells and on isolated fragments. For whole cells, a centrifuged pellet from a fluid culture was suspended in 1% tannic acid in 0.15 M phosphate buffer (pH 7.4) for 10 min, centrifuged, and then resuspended in 4% glutaraldehyde in the same buffer for 1 h. We then washed the cells three times in phosphate buffer before embedding the pellet in 2% Noble agar (Difco) and cutting it into 1-mm blocks. These blocks were processed as described previously (6): postfixed in 1% OsO_4 in Veronal buffer (pH 6.1), block stained in 0.5% uranyl acetate, dehydrated in acetone series, and embedded in Vestopal W. Sections were cut and stained with uranyl acetate and lead citrate. To prepare cell envelopes, cells were suspended in 1 mM $CaCl_2$–1 mM $MgSO_4$ and exposed to 20 kc of sonic oscillation in an MSE Ultrasonic apparatus for 5 s. The emptied envelopes were retrieved by differential centrifugation. These envelopes were then fixed in 4% glutaraldehyde in phosphate buffer (1 h), washed three times with buffer, stained with 1% uranyl acetate (1 h), dehydrated in ethanol series, and embedded in Epon 812 (Ladd Industries). All solutions up to 95% ethanol also contained 1 mM $CaCl_2$ and 1 mM $MgSO_4$. Sections were cut and stained as described above.

Negatively stained samples were prepared by mixing the sample suspension with 1% potassium phosphotungstate (pH 7). Carbon-Formvar–coated grids were then floated on drops of this mixture on dental wax to permit the material to become attached. Excess solution was then removed with bibulous paper before drying in vacuo. To prepare fragments of the RS layer suitable for negative staining, 24- to 48-h cultures (either from fluid medium or washed off solid medium) were suspended in 0.2% $CaCl_2$, 0.2% $MgCl_2$, and 0.1% NaCl and shaken with 0.2-mm glass beads vigorously by hand for 2 min. The cells and beads were sedimented by centrifugation (2,000 × *g* for 5 min), and then the wall fragments were isolated by centrifugation at 12,000 × *g* for 20 min.

To prepare samples for freeze fracture and etching, cells grown on solid medium (24 h at 30°C) were washed off with fluid medium containing 20% glycerol. The cells were then centrifuged, and portions of the pellet were frozen on copper disks in Freon 22 and stored in liquid nitrogen until required. Cleaving, etching, Pt-C shadowing, and replicating were carried out in a Balzers freeze-etch apparatus (Balzers AG, Liechenstein; model BA510M) as described previously (6).

Specimens were examined in Philips EM200 and EM300 electron microscopes at 60 kV, and images were recorded on Kodak 35-mm fine grain release positive film 5302.

Computer image processing. Conventional Fourier-based methods (reviewed, for example, in references 2 and 10) were employed to enhance the signal-to-noise ratio of the electron micrographs. In effect, these procedures average the information present in the image and so tend to even out spurious features. They also permit the data to be manipulated much more conveniently than is possible by simple photographic methods, and this can be very helpful when comparing different types of images as we wished to do here.

Areas of micrographs which were free of obvious imperfections were selected and examined by optical diffraction (10) to determine those in which the structure was well preserved to a resolution of better than 3 nm and in which the diffraction spots were strong compared to the background. The background was also examined to ensure that it was approximately symmetrical (indicating low astigmatism) and that the first minimum of the phase-contrast transfer function occurred at a frequency substantially higher than the highest frequency diffraction spots. This ensured that phase-reversal artifacts were absent. Only areas which met these rigorous and objective criteria were used for subsequent computer image processing. These areas were digitized on an Optronics P-1000 drum scanner or Perkin-Elmer PDS flat bed microdensitometer with a raster spacing corresponding to approximately 0.4 nm on the original object.

Subsequent processing was carried out on Control Data CYBER 73 or CYBER 76 computers, using software written in FORTRAN IV. Areas of 512 by 512 picture elements were boxed off from the density arrays, and their Fourier transforms were computed. The position of lattice points was determined by examining line printer representations of the transform amplitude matrix and structure factor amplitudes and phases obtained by integrating over small windows centered on the lattice points (16). Final filtered images were produced by Fourier inversion and were output either as density matrices on a line printer, as contour plots by using an Information International Inc. COMp80 microfilm device, or as continuous tone images on an Optronics Colorwrite C-4300 system.

Least-squares analysis. Least-squares analysis was employed to determine the parameters that gave the best correspondence between the observed ribbed pattern and that simulated from two overlapping hexagonal layers. For convenience, the analysis was carried out in Fourier space (as a consequence of Parseval's theorem, the values which give the best fit in Fourier space will also give the best fit in real space), using the structure factors given in Table 1. The simulated structure factors were produced by adding two sets of hexagonal layer structure factors (indexed, for convenience, on the *cmm* unit cell of the ribbed layer) after appropriate phase changes to reflect the relative positions of the layers [this reduced to a phase change of 180° for (h+k) odd for the *cmm* lattice for the structure factors of one of the layers, corresponding to a shift of one-half unit cell in the (1,0) direction]. The weight of each layer, and also a Gaussian point spread function to compensate for differences in lattice order between the images (15–17), were then computed so that the squared residual between predicted and observed structure factor sets was minimized. Details of the computing procedures employed have been described in detail elsewhere (15).

RESULTS

General appearance of the cell surface. Whole cells of *A. serpens* MW5 showed clear structure on the external surface of the cell wall. Negatively stained preparations showed linear banding (repeat frequency, 17 to 18.5 nm) along the length of the cell (Fig. 1). While subunits seemed

TABLE 1. Structure factors derived from computer Fourier analysis of areas of electron micrographs of negatively stained fragments of the RS layer of *A. serpens* MW5

Miller indices		Structure factors[a]			
For *p6mm* symmetry	For *cmm* symmetry	Hexagonal layer[b]	Ribbed layers		
			1	2	3
1,1	2,0	−433	−400	−432	−408
2,2	4,0	100	90	80	75
3,3	6,0	38	25	17	18
4,4	8,0	−28	−12	—	−17
0,1	1,1	890	90	151	153
1,2	3,1	−369	−60	−91	−75
2,3	5,1	75	−53	46	45
3,4	7,1	−28	−12	−10	−37
0,1	0,2	890	800	903	832
0,2	2,2	−248	−140	−172	−149
1,3	4,2	−82	−87	−134	−110
2,4	6,2	−47	−20	−15	27
3,5	8,2	−22	−10	−8	17
1,1	1,3	−433	−77	−145	−86
0,3	3,3	−83	—	−54	−58
1,4	5,3	−71	16	−54	−47
2,5	7,3	30	—	13	38
0,2	0,4	−248	−140	−300	−182
1,2	2,4	−369	−150	−275	−195
0,4	4,4	180	110	123	120
1,5	6,4	−44	−20	−25	−31
2,6	8,4	−27	—	−14	21
1,2	1,5	−369	−70	−135	−68
1,3	3,5	−82	−45	−55	−71
0,5	5,5	50	27	—	29
1,6	7,5	—	—	13	29
0,3	0,6	−83	−87	−184	−72
2,2	2,6	100	56	60	−70
1,4	4,6	−71	−53	−53	−75
0,6	6,6	—	−21	—	−29
1,7	8,6	—	—	16	—
1,3	1,7	−82	42	−43	−60
2,3	3,7	75	61	—	52
1,5	5,7	−44	—	−25	−32
0,7	7,7	−31	—	−30	−26
0,4	0,8	180	80	86	111
2,3	2,8	75	53	32	69
2,4	4,8	−47	−35	—	−33
1,6	6,8	—	—	26	24
1,4	1,9	−71	64	−47	−96
3,3	3,9	38	24	—	36
2,5	5,9	30	10	17	22
0,5	0,10	50	25	50	59
2,4	2,10	−47	—	−40	−33
3,4	4,10	−28	—	—	−23
1,5	1,11	−44	—	−31	28
3,4	3,11	−28	—	—	−28
0,6	0,12	—	—	—	−36
2,5	2,12	30	−12	−14	−26
4,4	4,12	−28	—	−14	25
1,6	1,13	—	—	—	27
3,5	3,13	−22	—	−26	−24
0,7	0,14	−31	—	—	−44

[a] After averaging data which the symmetry of the patterns (13) required to be equivalent. —, No measurement was made.

[b] Average of two areas.

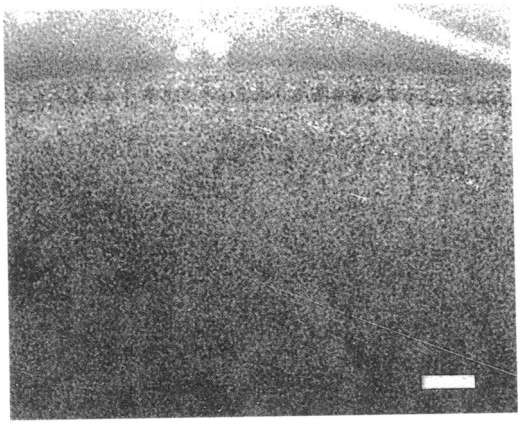

FIG. 1. Whole mount of an *A. serpens* MW5 cell negatively stained with potassium phosphotungstate, showing a distinct ribbed pattern. Bar, 50 nm.

to be present at the cell margin, they became indistinct in the body of the pattern, probably as a result of the superposition of patterns from the top and bottom of the cell. Most preparations also showed a thin continuous line outside the units at the outside edge of the cell wall. A similar linearity was apparent in shadowed replicas. The hemispherical ends of the cells showed a patchwork of different orientations. The ridges in most preparations (about 16 nm apart) seemed to lack sharpness, which may have been due to eutectic formation or to an outer covering on the RS layer. Occasionally areas having a hexagonal pattern were seen on a surface otherwise without structure. The spacing between these hexagonal units was about 17 nm.

Sections of whole cells (Fig. 2a) and of isolated envelopes (Fig. 2b) showed a repeating structure outside the outer membrane of the cell wall,

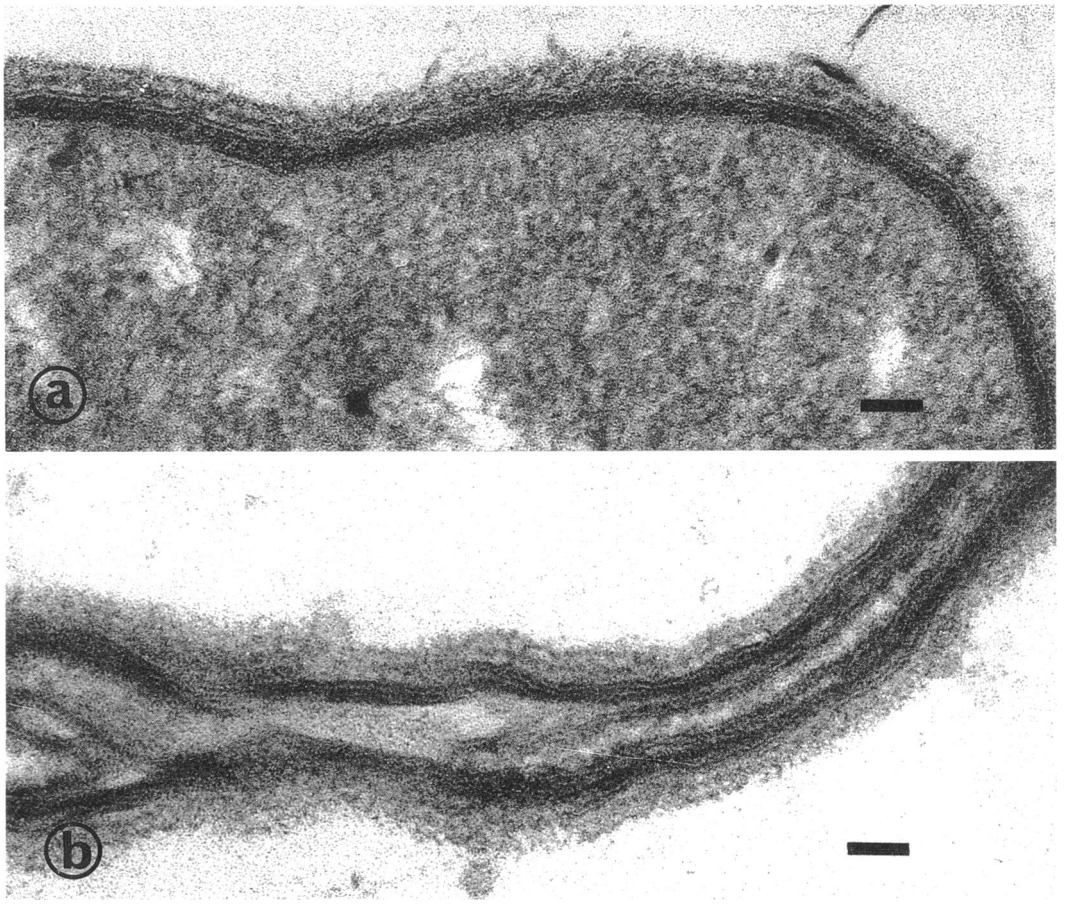

FIG. 2. Appearance of the RS layer of *A. serpens* MW5 in sectioned embedded material. (a) Whole cells; (b) isolated cell envelopes. When viewed from along the layer, two series of regular dark subunits can be seen. Bar, 50 nm.

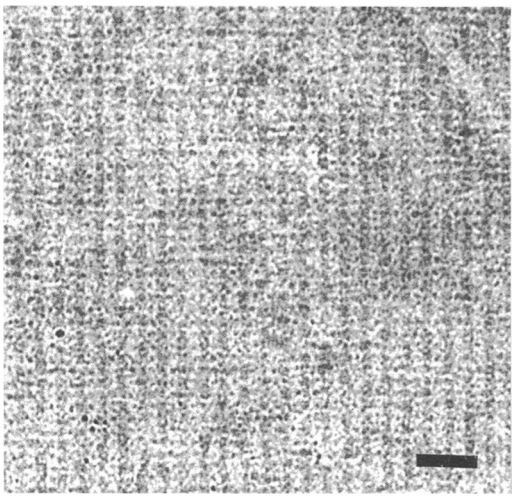

FIG. 3. Isolated sheets of the RS layer of *A. serpens* MW5 negatively stained with potassium phosphotungstate, showing the same pattern of ribs observed in whole-cell mounts. Bar, 50 nm.

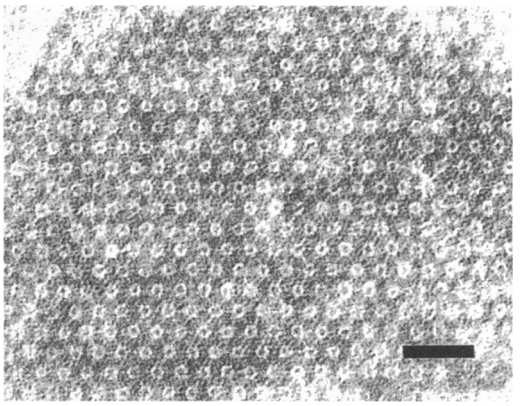

FIG. 4. Isolated fragment of the *A. serpens* MW5 RS layer showing a hexagonal pattern. Negatively stained with potassium phosphotungstate. Bar, 50 nm.

provided tannic acid was used in the fixation protocol or provided calcium and magnesium were maintained at 1% in all aqueous solutions used in fixation and dehydration. In these cases, the components of the RS layer were positively stained, as was evident in areas of tangential section. Where the section plane was normal to the RS layer, there appeared to be two distinct layers of repetitive structure outside the outer membrane. In some places, the subunits of these two layers appeared to alternate.

Two types of structure were commonly observed in isolated RS layer fragments. The first consisted of sheets showing a ribbed pattern (Fig. 3) similar to that observed on negatively stained whole cell mounts, which presumably represented patches disrupted from the cell envelope by the isolation procedure. In micrographs of isolated sheet material there were also sometimes small areas in which the dominant pattern of ribs was replaced by a hexagonal pattern (Fig. 4) resembling that seen on other *A. serpens* strains. In addition to these sheets, a tubular aggregate (Fig. 5) was also often seen, particularly in older cultures. These tubes resembled the structures sometimes seen in *A. serpens* VHA preparations (6–8, 12) and may have resulted from reassembly of the RS protein and some outer membrane lipids. Unfortunately, these tubes, like their counterparts from strain VHA (12), had cylindrical symmetry and so were not suitable objects for the Fourier-Bessel three-dimensional reconstruction techniques which have proved so effective on objects with helical symmetry (2, 10).

Structure of the layers. Computer image processing was employed to obtain a more quantitative representation of the structure of the layers. Suitable areas were digitized and processed by the usual Fourier-based methods to permit structure factors to be produced. These are the numerical values of the Fourier transform of the object at the positions corresponding to its lattice and are analogous to the peaks seen in an optical diffraction pattern. The structure factors were analyzed to establish the symmetry of the images and, for each image type, symmetry-related values were averaged to further enhance the signal-to-noise ratio and thus the reliability of the data.

Visual inspection suggested that the hexagonal layer fragments probably had sixfold symmetry, and this was confirmed by inspection of the position and phases of the peaks in the comput-

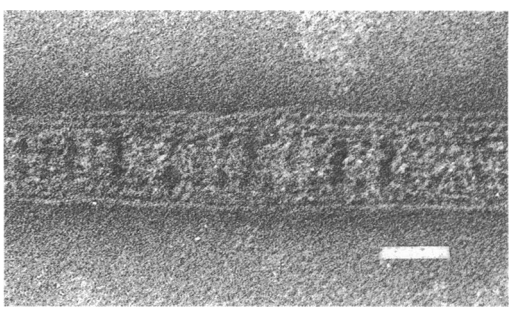

FIG. 5. Tubular aggregates often observed in preparations of RS layers isolated from *A. serpens* MW5. Negatively stained with potassium phosphotungstate. Bar, 50 nm.

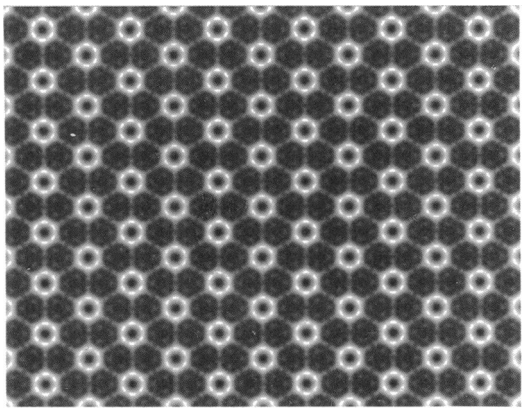

FIG. 6. Fourier filtered image of the hexagonal layer observed in negatively stained preparations of the *A. serpens* RS layer (e.g., Fig. 4). Note the presence of fine "delta" linkers between the annular units. The annuli are located on the sixfold axes of the *p6mm* unit cell, and the linkers are directed along the (1,0) lattice lines. Center-to-center distance is 18.5 nm (corresponding to a = 16 nm in the *p6mm* unit cell).

ed Fourier transforms. The peaks were arranged on a regular hexagonal lattice with a = 16 nm, and, for an appropriate phase origin (located on a sixfold axis at the center of each annulus), all structure factor phases were within a few degrees of either 0 or 180°, which is the condition required for *p6* symmetry (13). Detailed inspection of the structure factor amplitudes indicated that they were consistent with the higher *p6mm* symmetry [**F**(h,k) = **F**(k,h)]. The structure factors were averaged accordingly, and final values, obtained by combining data from two areas, are given in Table 1. A filtered image is shown in Fig. 6, where the central annulus and six radiating delta linkers directed along the (1,0) lattice lines of the *p6mm* unit cell are clearly visible.

Areas of three micrographs of negatively stained layers which had the ribbed conformation were also processed by computer methods. The peaks in their Fourier transforms were located in the same positions as were the peaks in the transforms from the *p6mm* hexagonal layers, but the intensities were different. As would be expected from the general appearance of the images, there was no evidence for hexagonal symmetry, and the pattern was indexed on a rectangular lattice with unit vectors corresponding to 32 and 18.5 nm. The clear absence of lattice points when (h+k) was odd implied the presence of glide planes in the images and probably a center of symmetry. For an appropriate phase origin all structure factor phases were within a few degrees of 0 or 180°, and detailed examination of the structure factor amplitudes confirmed that they obeyed the requirements (13) for the centric symmetry group *cmm* [**F**(h,k) = **F**(−h,k) for (h+k) even, and **F**(h,k) = 0 for (h+k) odd]. Table 1 gives the structure factors, after internal averaging appropriate to *cmm* symmetry, for the areas processed. Because there appeared to be distinct differences between the values from the different images, it was thought unwise to average between images (at least until the source of variation was identified), and so these were treated separately in subsequent processing. Filtered images were obtained by Fourier inversion and are shown in Fig. 11.

Moiré structure. Consideration of the patterns obtained from both types of layer indicated that the ribbed structure might have been produced by the superposition of two hexagonal layers, possibly with some additional material also present. A number of observations indicated that the RS material from strain MW5 was a multilayered structure. There appeared often to be two layers present in micrographs of embedded sectioned material (Fig. 2), and furthermore, objects such as that shown in Fig. 7 were occasionally seen in negatively stained tube preparations and probably represent an end-on view of a small length of the tube. In these images two layers can be clearly seen. Two layers would also be consistent with the observation that the lattice points for each type of image were in the same position in the computed Fourier transforms. Because addition is linear under Fourier transformation, the Fourier transform of the sum of two *p6mm* hexagonal layers is the same as the sum of the transforms of the two individual layers (after appropriate phase changes to reflect the relative positions of the layers). Therefore, the Fourier transform of the two superimposed hexagonal layers would be expected to have lattice points in the same positions as a single hexagonal layer, but with different structure factor amplitudes

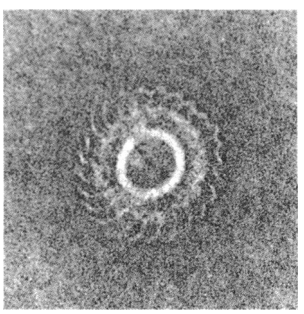

FIG. 7. Particle occasionally seen in negatively stained material isolated from the *A. serpens* MW5 RS layer and presumed to represent an end-on view of the tubular aggregates illustrated in Fig. 5.

and phases because the phase shift for each lattice point in the sum will be different (and will depend on the relative position of the two hexagonal layers).

This hypothesis was investigated by detailed analysis of the results obtained by computer image processing. Cross-correlation analysis was employed first to determine whether there was any significant relationship between the two images in addition to their sharing common lattice point positions in their computed Fourier transforms. In essence, this procedure determined the degree of correspondence between the two images as one was moved relative to the other, and in this way a two-dimensional map was built up. A typical example is shown in Fig. 8, in which there are clearly two regular series of maxima in the cross-correlation map between a single hexagonal layer and a ribbed pattern. This strongly supported the notion that the ribbed layer derived from the superposition of two hexagonal layers. The cross-correlation maps indicated that the second layer was displaced by half a repeat along a hexagonal (1,0) lattice line relative to the first. Figure 9 illustrates how this could produce the ribbed appearance by the close apposition of the central annuli of the two hexagonal layers, whereas Fig. 10 shows an area from a micrograph of a negatively stained RS layer fragment which bears a striking resemblance to Fig. 9, with a section of ribbed pattern flanked by two areas of hexagonal pattern which are shifted relative to one another. However, the simulated pattern in Fig. 9 was different in detail from the observed patterns (Fig. 11), and fur-

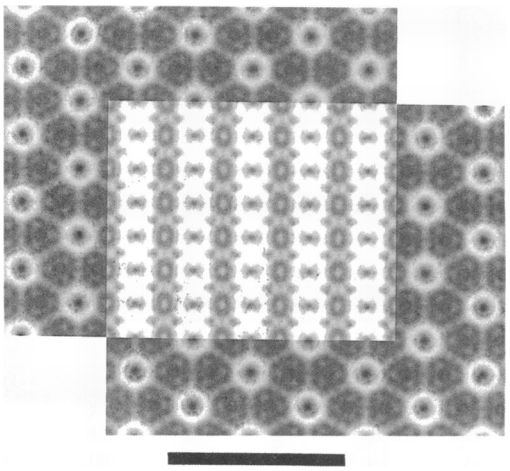

FIG. 9. Illustration of how a ribbed pattern could be derived from a translational moiré involving two hexagonal layers placed so that one is shifted half of a repeat (9.25 nm) relative to the other along a (1,0) lattice line. In this idealized representation both layers have the same density, but in practice, the densities of the two hexagonal layers appear to be different, probably as a result of uneven negative staining. Bar, 50 nm.

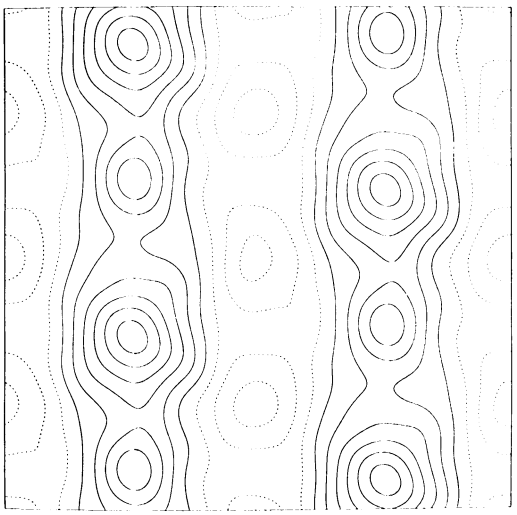

FIG. 8. Cross-correlation map between a single *p6mm* hexagonal layer and the *cmm* ribbed layer. Note the presence of two series of maxima (indicative of correspondence between the patterns), which implies that the ribbed layer pattern is the result of a translational moiré between two hexagonal layers. The relative positions of the two sets of maxima indicate that one hexagonal layer in the moiré is translated by half of one repeat along a (1,0) lattice line (in the *p6mm* unit cell) relative to the other.

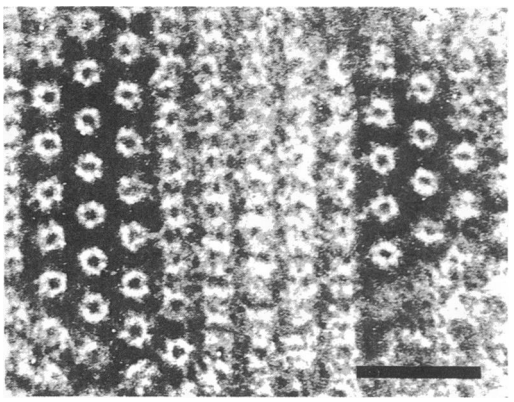

FIG. 10. Micrograph showing hexagonal areas on either side of a ribbed layer. Note that the layer on one side is shifted by one half repeat along a (1,0) lattice line relative to that on the other. The analogy between this observed image and the simulated image (Fig. 9) is striking and suggests very strongly that the ribbed pattern results from the superposition of the densities of the two hexagonal layers. Bar, 50 nm.

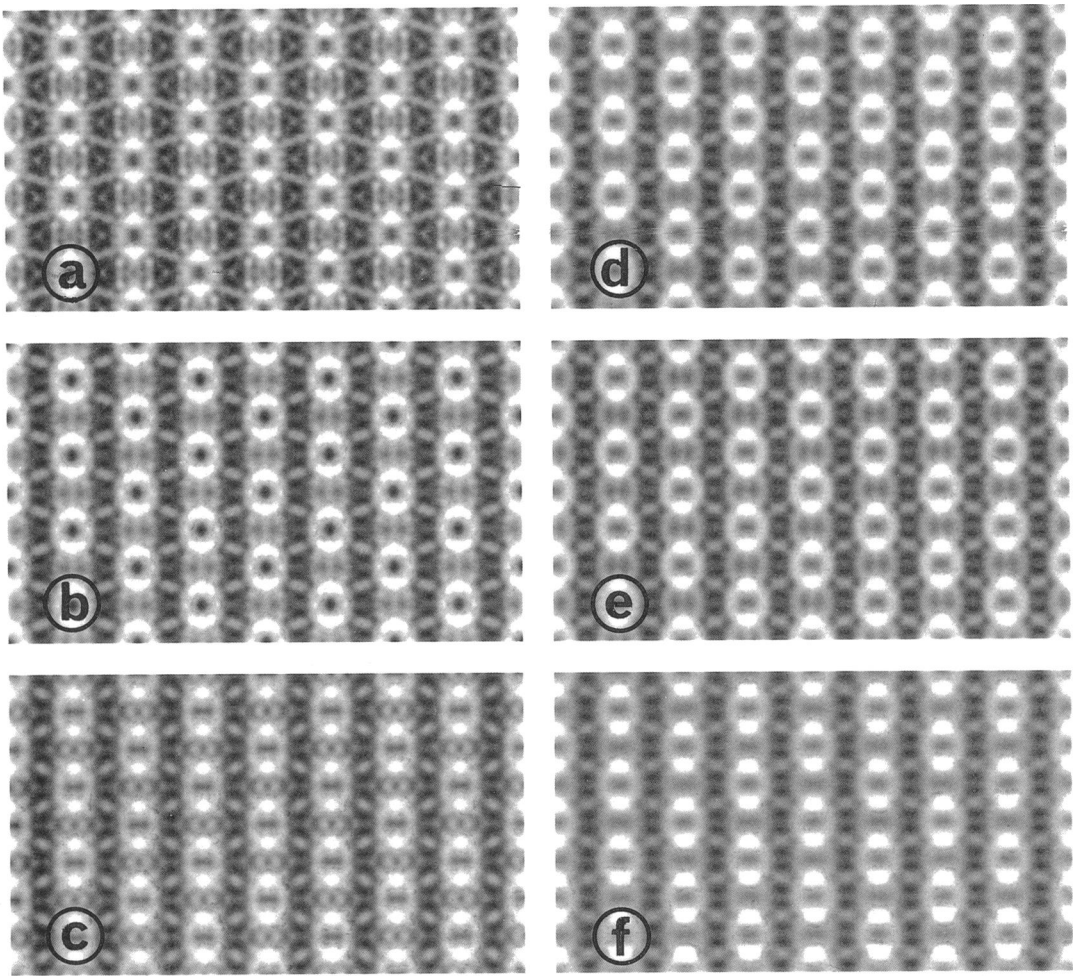

FIG. 11. Observed and predicted images of the ribbed layer. Images (a) to (c) are Fourier-filtered images based on the structure factors (Table 1) derived from three different areas of micrographs showing the ribbed pattern. Images (d) to (f) are simulations based on two overlapping hexagonal layers, using the weighting parameters determined by the least-squares analysis. The correspondence between predicted and observed images is remarkably good, and images showing the density difference between predicted and observed patterns showed no systematic pattern. Spacing between ribs corresponds to 16 nm.

thermore, two hexagonal layers overlapping in this manner should produce a composite image with *pmm* symmetry, with $a = 16$ and $b = 9.3$ nm, instead of the *cmm* symmetry observed. In other words, for the image simulated in Fig. 9, many of the peaks observed in the Fourier transforms of the ribbed layers should have been absent: if *cmm* indexing is retained, all structure factors with either h or k odd should have been zero. Inspection of the structure factors (Table 1) indicated that these structure factors were generally considerably weaker than those for which h and k were even, but the power contained in these "forbidden" *pmm* reflections was still appreciable and could not be ignored.

This discrepancy probably arose from the two layers being stained unequally. This is a very common occurrence in negatively stained material and here it would make the Fourier transform of one layer stronger than that of the other. Therefore contributions from each transform would not cancel exactly at the "forbidden" lattice points and so this would explain the observed transforms. It would also be consistent with the cross-correlation results in which the peaks in the map (Fig. 8) were clearly stronger

for one layer than for the other. A quantitative least-squares analysis was undertaken to ascertain the extent to which the observed ribbed patterns could be explained by this hypothesis. This enabled us to make an objective assessment of the relative staining intensities of the layers and also to compensate for differences in lattice disorder between the layers. A very close correspondence was obtained between the predicted and observed patterns, indicating that this model did provide a satisfactory explanation both for the ribbed pattern in general and also for the differences observed between the filtered images. The residual sums of squares for the three images investigated represented, respectively, 7.1, 4.7, and 3.9% of the image power, which was of the same order as the errors expected in the data. The close agreement between predicted and observed structures is further illustrated in Fig. 11, which shows, for each area investigated, the image produced by Fourier inversion of the observed pattern and that predicted by the least-squares analysis. Furthermore, there was no consistent pattern in the difference maps (obtained by subtracting simulated from observed), which was consistent with their being random and due primarily to errors in the measurement of the exact values of the various structure factors.

DISCUSSION

The results obtained from the least-squares analysis demonstrated conclusively that the ribbed pattern observed on the *A. serpens* MW5 RS layer resulted from the superposition of two hexagonal *p6mm* layers as illustrated in Fig. 9. The close correspondence between the patterns simulated on this basis and those actually observed, combined with the random nature of the density differences between them in the areas examined, indicated that there was no need to propose the presence of extra material to account for the ribbed pattern. This does not, of course, exclude the presence of extra material in the layer, but it does mean that, in projection, any such additional material must be essentially featureless. One possible indication of the presence of extra material was the distinct line seen outside the rolled margin of whole-cell mounts (Fig. 1) or at the edge of the tubular assemblies seen in old cultures (Fig. 5), but this appearance could easily have resulted from the superposition of linkers in this view. Although a similar line is not seen in the analogous tubes formed from *A. serpens* VHA, this is probably due to this strain having Y linkers instead of the delta linkers of the MW5 hexagonal layers. The view that the line in the tubular aggregates is a superposition artifact and not a third layer was supported by the end-on views of these aggregates (Fig. 7) in which only the material from the two hexagonal layers could be seen.

We were not able to obtain a definitive answer as to the orientation of one layer relative to the next in the direction perpendicular to the plane of the layer. The end-on views of the tubular aggregates (Fig. 7) suggested that both layers were oriented in the same direction, with the cylinders (which are seen as annuli in projection) innermost and the linkers facing the exterior, as is probably also the case in the analogous hexagonal layer in *A. serpens* VHA (12). However, since the tubes probably resulted from reassembly of the RS layer protein and also because the exact register of the two layers cannot be the same here as in sheets (since, as a result of the curvature of the layer, there are fewer units in the inner layer and so their register with the outer layer must be continually changing, at least in a circumferential direction), it may not be valid to extrapolate from this aggregate to the structure of the RS layer on the bacterium.

The structure determined for the MW5 RS layer was consistent with the concept of a selective protective barrier recently proposed as a general function of these layers (16, 17). The gaps in a *p6mm* hexagonal layer would generally be expected to obstruct the passage of molecules larger than about 2 nm (such as lytic enzymes) while still enabling the passage of nutrients and waste products into and out of the cell. In this respect, the linkers between the cylinders in the layer may serve to limit the size of the gaps in the layer in addition to any role they may have in the mechanical stability of the layer. It is not, however, immediately clear how the presence of the second layer would improve this protective function, and it could be that the second layer is instead related to one of the other roles of the RS layer. The presence of the second layer would, for example, greatly increase the effectiveness of the layer in protecting the cell from deleterious environmental agents such as heavy metals (see reference 3).

An interesting feature of the structure of the MW5 RS layer is that while the underlying hexagonal layer is attached to the lipopolysaccharide of the cell outer membrane, the second hexagonal layer appears to be attached directly to the first. Thus it would appear that the same molecule is involved here in two different types of structural interaction. Of course, this assumes that the two layers are identical in structure and this may not be the case: although we were unable to detect any consistent difference between the upper and lower hexagonal layers, our study was limited to 2.5-nm resolution and so would not be expected to pick up subtle structural differences. Thus, for example, there could easily be a slight difference in either the cylindri-

cal units or the linkers in one layer which would account for its interacting in a slightly different manner from the other. Alternatively, the two layers could be identical and the second simply results from the production, by the cell, of an excess of RS protein. Certainly other species form excess RS protein (14, 18).

Finally, the observation that the ribbed RS layer of *A. serpens* MW5 was actually a composite of two hexagonal layers resolved the difficulty which this pattern posed in respect to the patterns observed in other strains of this organism: the *A. serpens* RS layers can now be understood as all arising from similar proteins packed in a very similar manner and having a common structure of hexagonally arranged cylinders connected by fine linkers.

ACKNOWLEDGMENTS

We are grateful for the support, both for research and for working visits (for M.S.), provided by the Medical Research Council of Canada and the Academic Development Fund of the University of Western Ontario.

The technical assistance of M. Hall, H. Koppenhoeffer, J. Marak, and P. Cohen was of inestimable value. We are also most appreciative of the involvement of many of our colleagues and of their helpful comments, criticisms, and assistance. Particularly, among those who were intrigued and puzzled by this complex structure and who struggled with us to resolve it, we would like to thank George Hageage, Sigmund Maier, Francis Buckmire, Terrance Beveridge, and Don Fraser.

LITERATURE CITED

1. **Aebi, U., P. R. Smith, J. Doubochet, C. Henry, and E. Kellenberger.** 1973. Structure of the regular T-layer of *Bacillus brevis*. J. Supramolec. Struct. **1**:498–522.
2. **Amos, L. A.** 1974. Image analysis of macromolecular structures. J. Microsc. **100**:143–152.
3. **Beveridge, T. J.** 1981. Ultrastructure, chemistry and function of the bacterial cell wall. Int. Rev. Cytol. **72**:229–317.
4. **Beveridge, T. J., and R. G. E. Murray.** 1975. Surface arrays on the cell wall of *Spirillum metamorphum*. J. Bacteriol. **124**:1529–1544.
5. **Buckmire, F. L. A.** 1971. The physical structure of the cell wall as a differential character. Int. J. Syst. Bacteriol. **20**:345–360.
6. **Buckmire, F. L. A., and R. G. E. Murray.** 1970. Studies on the structure of the cell wall of *Spirillum serpens*. Can. J. Microbiol. **16**:1011–1022.
7. **Buckmire, F. L. A., and R. G. E. Murray.** 1973. Studies on the structure of the cell wall of *Spirillum serpens*. Can. J. Microbiol. **19**:59–66.
8. **Buckmire, F. L. A., and R. G. E. Murray.** Structure and in vitro assembly of the outer, structural layer of *Spirillum serpens*. J. Bacteriol. **125**:290–299.
9. **Chester, I. R., and R. G. E. Murray.** 1978. Protein-lipid-lipopolysaccharide association in the superficial layer of *Spirillum serpens* cell wall. J. Bacteriol. **133**:932–941.
10. **Crowther, R. A., and A. Klug.** 1975. Structural analysis of macromolecular assemblies by image reconstruction from electron micrographs. Annu. Rev. Biochem. **44**:161–182.
11. **Finch, J. T., A. Klug, and M. V. Nermut.** 1967. The structure of the macromolecular units on the cell wall of *Bacillus polymyxa*. J. Cell Sci. **2**:587–590.
12. **Glaeser, R. M., W. Chiu, and D. Grano.** 1979. Structure of the surface layer protein of the outer membrane on *Spirillum serpens*. J. Ultrastruct. Res. **66**:235–242.
13. **Henry, N. F. M., and K. Lonsdale** (ed.). 1969. International tables for X-ray crystallography, p. 65–66. Kynoch Press, Birmingham, England.
14. **Sleytr, U. B.** 1978. Regular arrays of macromolecules on bacterial cell walls. Int. Rev. Cytol. **53**:1–64.
15. **Stewart, M.** 1981. The structure of alpha-tropomyosin magnesium paracrystals. II. Simulation of staining patterns from the sequence and some observations on the mechanism of positive staining. J. Mol. Biol. **148**:411–425.
16. **Stewart, M., and T. J. Beveridge.** 1980. Structure of the regular surface layer of *Sporosarcina ureae*. J. Bacteriol. **142**:302–309.
17. **Stewart, M., T. J. Beveridge, and R. G. E. Murray.** 1980. Structure of the regular surface layer of *Spirillum putridiconchylium*. J. Mol. Biol. **137**:1–8.
18. **Thorne, K. J. I.** 1977. Regular arrays of protein on the surfaces of Gram negative bacteria. Biol. Rev. **52**:219–234.